Research Square

Preprints are preliminary reports that have not undergone peer review.
They should not be considered conclusive, used to inform clinical practice,
or referenced by the media as validated information.

First Geodetic Documentation of Progressive Crustal Deformation Reversal Over 15 Years Following the 2011 Mw 9.1 Tohoku-Oki Earthquake

Xiaolong Zhang
CAS Institute of Geology and Geophysics: Institute of Geology and Geophysics Chinese Academy of Sciences
Shaoyang Li
shaoyangli@mail.iggcas.ac.cn
Institute of Geology and Geophysics Chinese Academy of Sciences https://orcid.org/0000-0001-9832-4561
Ling Chen
CAS Institute of Geology and Geophysics: Institute of Geology and Geophysics Chinese Academy of Sciences

Research Article

Keywords: 2011 Tohoku-Oki earthquake, Postseismic deformation, Crustal deformation reversal, Reversal time, Reversal duration, GNSS

Posted Date: November 20th, 2026

DOI: https://doi.org/10.21203/rs.3.rs-11601446/v1

License: This work is licensed under a Creative Commons Attribution 4.0 International License. Read Full License

Abstract

Following a giant subduction earthquake, continental surface motion is expected to reverse from seaward to landward as postseismic transients decay and the megathrust relocks. This reversal has so far been reconstructed only piecemeal from snapshots of different margins in different earthquake-cycle phases, never observed continuously in space and time at a single margin, hindering efforts to model the long-term deformation of the subduction system. Using more than 15 years of dense GNSS observations, and deliberately retaining the secular trend, we map this reversal for the first time following the 2011 Mw 9.1 Tohoku-Oki earthquake. The reversal initiates within one year in southern Hokkaido and southeastern Chubu-Kanto and propagates toward central Tohoku as two fronts advancing at 19.2 and 13.3 km/yr from the south and north, forming an arcuate boundary deflected toward the trench above the rupture. Both fronts decelerate with time, and stations that reverse later take proportionally longer to complete the switch to landward motion. The transition is also mildly asymmetric, with the seaward velocity decaying to zero somewhat more abruptly than landward motion subsequently builds up. Systematic north-south offsets in propagation rate and reversal duration reveal distinct temporal characteristics of surface-deformation recovery in the northern and southern segments. These observations provide new margin-scale constraints on the evolving balance between postseismic transients and renewed megathrust loading, and quantitative benchmarks for future coupled models of megathrust recovery.

1 Introduction

Following a giant megathrust earthquake, surface deformation reflects the evolving contributions of afterslip, viscoelastic relaxation, and the gradual recovery of interseismic loading (Wang et al., 2012; Govers et al., 2018; Sun et al., 2018; Li & Chen, 2023). These processes have been extensively investigated after the 2011 Tohoku-Oki earthquake (Fig. 1), yet one fundamental observational quantity remains poorly characterized: when and where does the long-term surface motion transition from seaward to landward across an entire subduction margin? Resolving this transition requires observations sufficiently long to capture the crossover between rapidly decaying postseismic deformation and much longer-lived landward motion.

In 2011, the Mw 9.1 Tohoku-Oki earthquake ruptured an approximately 500x300 km2 portion of the plate interface along the eastern Japan Trench (e.g., Simons et al., 2011; Wang et al., 2018; Uchida & Bürgmann, 2021; Toda & Stein, 2022) (Fig. 1). A dense Global Navigation Satellite System (GNSS) network across the entire country (Sagiya, 2004) revealed pervasive seaward motion immediately after the event across the entire Honshu Island (e.g., Ozawa et al., 2012; Nishimura, 2014). In contrast, enhanced landward motion (i.e., faster motion than before the 2011 earthquake) has been observed in adjacent segment on Hokkaido Island (Heki & Mitsui, 2013) (Fig. 1), a phenomenon which is later confirmed by many other great megathrust earthquakes (e.g., Melnick et al., 2017; Yuzariyadi & Heki, 2021). Such faster motion is consistent with seafloor GNSS-A observations immediately above the rupture zone in Japan Trench that are also significantly faster than the long-term subduction rate of the Pacific plate (e.g., Watanabe et al., 2014; Tomita et al., 2017; Honsho et al., 2019) (Fig. 1). It remains largely unknown whether these extra fast motions in the ruptured zone and adjacent segments share a common mechanism.

The onshore crustal deformation reversal, particularly near the arc region, could be a diagnostic indicator of an overall relocked megathrust, because locking is the only mechanism that can produce landward motion at such large distances from the trench, whereas afterslip along the megathrust interface and postseismic viscoelastic relaxation in the mantle wedge mainly produce seaward motion (Wang et al., 2012; Govers et al., 2018). Snapshots of such reversed deformation, from the coast to the arc region, have been documented in southern Chile (Klotz et al., 2001; Khazaradze et al., 2002) and Alaska (Suito & Freymueller, 2009). However, the dynamic reversal of crustal deformation across the entire upper plate has never been documented at any single margin, owing to the limited length of instrumental records (Li & Chen, 2023). The timing and spatial evolution of crustal deformation reversal along the Japan Trench therefore offer a further constraint on the megathrust locking state and on the decay of postseismic transients in the rupture zone, and may help to clarify the deformation processes along the adjacent segments.

In this study, in contrast to previous work that focused on short-term (a few years) and/or purely postseismic deformation, with the potential locking/secular signal purposely removed (e.g., Sun et al., 2014; Freed et al., 2017; Agata et al., 2019; Fukuda & Johnson, 2021; Dhar & Muto, 2023; Dhar et al., 2025), we extend the GNSS time-series analysis of the dense network to over 15 years and deliberately do not detrend the time series, in order to capture the timing of the true crustal deformation reversal. Here we address an explicitly observational question: how has the transition from seaward to landward surface motion evolved spatially and temporally during the first 15 years after the Tohoku-Oki earthquake? We quantify station-by-station reversal times and transition durations, map their margin-scale spatial evolution, and characterize the contrasting northern and southern patterns. These quantities constitute observational constraints that any physical model of long-term postseismic recovery should reproduce. Throughout this study, the term ‘reversal front’ refers exclusively to the migrating zero-velocity contour in the surface-deformation field and does not imply a directly resolved propagating boundary of megathrust relocking at depth.

2. GNSS Data Analysis

2.1 Trajectory Fitting of GNSS Time Series

We obtain daily final solutions of GNSS data defined in the Okhotsk-plate-fixed reference frame, processed by the Nevada Geodetic Laboratory (http://geodesy.unr.edu/index.php, last accessed 04/29/2026) (Blewitt et al., 2018). We download time series for all available stations within the latitude range of 33°N to 46°N and the longitude range of 138°E to 146°E (Fig. 2). Stations in southwestern Japan are excluded because they belong to a different subduction system and their deformation is not directly related to the postseismic processes along the Japan Trench. We apply a time series analysis approach to improve the quality and temporal continuity of the records from March 12, 2011, to April 11, 2026, following the strategy of our previous studies of postseismic deformation (e.g., Li et al., 2017; Zhang et al., 2025).

Before trajectory fitting, we correct discontinuities associated with earthquakes and antenna offsets. Earthquake steps with Mw > = 6 are taken from United States Geological Survey catalogue and associated stations are calculated using $D \leq 10^{(0.5M_w-0.8)}$ km, where *D* is the epicentral distance, *Mw* is the event moment magnitude. Antenna offsets are obtained from GSI maintenance records (https://terras.gsi.go.jp/denshi_hosyu.php), with additional manual corrections applied where documented. Then, we model the displacement time series of each station using ordinary least squares with a linear trend, a logarithmic transient, annual and semiannual terms (Bevis & Brown, 2014) as follows:

$$x(t) = c + Vt + A_{\log}\ln\left(1 + \frac{t}{\tau_{\log}}\right) + a_1\cos(2\pi t) + b_1\sin(2\pi t) + a_2\cos(4\pi t) + b_2\sin(4\pi t)$$

1

where t is time in years relative to the Tohoku-Oki earthquake, V is the linear rate, $A_{\log}$ is the logarithmic amplitude, and $\tau_{\log}$ is the logarithmic timescale. The $\tau_{\log}$ is estimated by grid search over 0.1–5.0 years at 0.1-year intervals. For each candidate timescale, the remaining linear parameters are solved by least squares, and the timescale yielding the minimum root-mean-square (RMS) residual is selected. Residual outliers are screened using a criterion of 4 times median absolute deviation method. The RMS residual is used to evaluate the fit quality at each station. Model performance is assessed by examining the unmodeled residuals across all stations, which are close to zero mm (Figure S1). This fitting procedure improves the precision with which the reversal time and reversal duration can subsequently be estimated.

The seasonal terms are excluded when calculating tectonic velocity, whereas the linear and logarithmic components are retained together (Figure S2a) to represent the fitted nonseasonal tectonic trajectory, attributed jointly to afterslip, viscoelastic mantle relaxation, and megathrust relocking (Li et al., 2017, 2018). Importantly, rather than prescribing the logarithmic function solely as a transient postseismic signal and the linear function solely as a preseismic secular rate or relocking signal, we allow both functions together to represent the full tectonic deformation, thereby relaxing the assumption of immediate relocking commonly adopted in previous studies. Despite certain trade-offs among the parameters of the linear and logarithmic functions, this approach is expected to improve the signal-to-noise ratio of the fitted tectonic trajectory relative to the raw GNSS observations (Figure S2a). A comparison with a quadratic function yields similar reversal times within the observation period, as discussed in Section 4.1 (Figure S13). Based on the combined linear and logarithmic functions, we reconstruct the systematic and continuous evolution of east-component displacement velocities at all 426 GNSS stations across the margin (Fig. 2), as deformation along this margin is dominated in the east-west direction (e.g., Ozawa et al., 2012; Nishimura, 2014; Sun et al., 2014; Iinuma et al., 2016; Fukuda & Johnson, 2021; Dhar & Muto, 2023).

2.2 Estimate of Reversal Time and Reversal Duration in East-component Displacements

From these tectonic functions, we then estimate the reversal time (tr) and reversal duration (tmax minus tmin) at each station from its east displacement component (Figs. 2, S2b and S2c). We use the east component because the postseismic deformation across the study region is dominated by east-west motion (e.g., Ozawa et al., 2012; Nishimura, 2014; Sun et al., 2014; Iinuma et al., 2016), and a single fixed reference direction allows the reversal timing to be compared consistently among all stations. The trench is not perfectly linear: it strikes nearly north-south along Tohoku and Kanto but bends toward the northeast off Hokkaido, so that the trench-normal direction and the station-to-trench geometry vary along the margin (Figure S3). This variation is concentrated in the north, where the obliquity between the plate convergence and a fixed east-west reference is largest. Critically, however, these obliquely convergent stations in northeastern Hokkaido are precisely those dominated by enhanced landward motion that exhibit no directional reversal throughout the observation period (Heki & Mitsui, 2013), and therefore contribute no reversal times that the projection could bias. The reversal fronts we document are confined to the Tohoku-Kanto region (Figs. 2 and 3), where the trench is comparatively uniform and the convergence is nearly trench-normal, so that the east-component zero crossing faithfully captures the seaward-to-landward reversal of the full horizontal motion.

The reversal time tr is defined as the time elapsed since the Tohoku-Oki earthquake at which the east displacement velocity equals zero (Figure S2b). To estimate the reversal duration, we adopt a displacement threshold of 1 mm and define it as the time elapsed from when the station's cumulative westward displacement decreases to within 1 mm of zero velocity to when the station's cumulative eastward displacement exceeds 1 mm past zero velocity (Figure S2c). This threshold is preferred as the reference value because it is similar to the GNSS horizontal observation error and we evaluated 1–3 mm in sensitivity tests. This duration is a model-derived, threshold-dependent measure of the width of the reversal transition and should not be interpreted as a formal statistical uncertainty in tr. This approach extracts additional temporal information about how rapidly the station decelerates (i.e., pre-reversal span, tr minus tmin) and subsequently accelerates through the reversal (i.e., post-reversal span, tmax minus tr) (Figure S2c). A few typical time series fitting and estimate of reversal time and reversal duration are shown in Figure S4. Varying the displacement threshold has a negligible effect on reversal time but systematically changes the estimated reversal duration. These sensitivity tests are discussed in Section 4.1 (Figures S13 and S14). Together, the reversal times and durations estimated at more than 200 stations, along with the locations of more than 200 unreversed stations, constitute an unprecedented observational dataset for investigating the spatiotemporal evolution of megathrust kinematics following the giant Tohoku-Oki earthquake.

3. Results & Discussion

3.1 Inward-Propagating and Decelerating Reversal Fronts North and South of the Rupture

The GNSS network reveals a time-dependent reversal of horizontal surface displacement from seaward to landward motion following the Tohoku-Oki earthquake, with a systematic spatial distribution of reversal times and unreversed stations across the study region (Figs. 2, 3a and 3b). The results show that the reversal initiates very rapidly (< 1 year) after the earthquake simultaneously in southern Hokkaido District and in southeastern Chubu and Kanto

Districts, and then both progressively propagate toward the central Tohoku District over the 15 years following the 2011 earthquake, with the central part of this District still featuring unreversed seaward postseismic motion (Figs. 2, 3a and 3b). The propagation boundary thus forms an arcuate geometry whose central portion is deflected toward the trench and the 2011 rupture zone relative to the northern and southern regions. These observations suggest that the majority of the affected megathrust interface at both its northern and southern edges has regained its locked state, including the south area that featured strong afterslip immediately after the earthquake (e.g., Ozawa et al., 2012; Iinuma et al., 2016; Freed et al., 2017; Fukuda & Johnson, 2021) and little or no detectable afterslip in recent years (Watanabe et al., 2021), probably due to the subduction of seamount chain (e.g., Wang et al., 2018), and the north region that hosted the recent burst of megathrust events (e.g., Zhang et al., 2026; Yoshida et al., 2026) (Figs. 1 and 3a).

A planar fit to the reversal years describes a coherent propagation front for each region, with the front advancing toward 352° from north (black open arrow in Fig. 3a) at 19.2 km/yr (R2 = 0.88; Fig. 3b) for the southern stations and toward 228° from north (Fig. 3a) at 13.3 km/yr (R2 = 0.77; Fig. 3b) for the northern stations. Residuals of these fits are small at most stations (generally within ± 4 year; Fig. 3c), indicating that the reversal timing is well represented by overall-uniform along-axis propagation. The residuals nonetheless show systematic spatial structure. Both the northern and southern stations exhibit positive residuals near the leading edge of the propagation front (Figs. 3b and 3c), where the reversal occurs later than the uniform-velocity fit predicts, suggesting a margin-wide deceleration of the front with time after the earthquake. The southern stations additionally show a complex spatial pattern of residuals (Fig. 3c), with positive residuals in the central part of the region, where the reversal is relatively later. This pattern may suggest competing deformation processes associated with the triple-junction region (the Japan Trench, the Sagami Trough, and the Nankai Trough) that locally delay or accelerate the front.

The local propagation rates range from near 0 to about 40 km/yr and decrease systematically as the front advances in both the northern and southern regions (Fig. 3d), consistent with the deceleration inferred from the residuals (Fig. 3c). The local directions converge consistently toward central Tohoku from both the north and the south (Fig. 3d). Together, these rates and directions suggest that complete deformation reversal across the entire Honshu Island may take a few more decades, considerably longer than predicted by some numerical models (Sun et al., 2018; Li & Chen, 2023). To illustrate one possible continuation of the observed pattern, we extrapolate the preferred empirical trajectories to stations that have not reversed by 2026. Under the linear-plus-logarithmic formulation, many of these stations do not reach zero velocity for several decades and the front advances only a few tens of kilometers over the following two decades (Figures S5 and S6). However, Section 4.1 shows that extrapolated reversal times become strongly dependent on the assumed functional form outside the observation interval. We therefore regard Figure S6 as a model-dependent scenario rather than a robust prediction of future reversal timing.

3.2 Gradual and Asymmetric Reversal Durations North and South of the Rupture

The deformation reversal occurs as a gradual transition rather than an instantaneous switch, and both the pre-reversal and post-reversal time spans lengthen toward the leading edge of the propagation front (Fig. 4). The pre-reversal span (tr - tmin) measures how gradually the seaward velocity decays toward zero, whereas the post-reversal span (tmax - tr) measures how gradually the station subsequently builds up landward motion. The reversal duration therefore brackets the reversal time with lower and upper bounds and an associated uncertainty (Figure S2), and the location of the reversal time within this interval reflects the competition between the waning seaward postseismic transient and the strengthening landward signal of megathrust relocking. In map view, both spans are shortest (near 0 to 1 year) in the regions where the reversal initiated earliest and longest (up to about 4 year) in the regions that reversed latest, for the northern and southern stations alike (Figs. 4a and 4b). Along the propagation axis, the pre-reversal span increases with distance for both the northern and southern stations, from less than 1 year near the trailing edge to about 3 to 4 year near the contemporary front, with the northern stations systematically larger than the southern stations at a given distance (Fig. 4c). The post-reversal span shows the same increasing relationship with distance and the same north-south offset, reaching about 2 to 2.5 year near the front (Fig. 4d).

Reversal duration across all stations shows a clear linear relationship with reversal time (Figs. 4e and S7), suggesting that both quantities are governed by similar competing processes operating consistently across the entire margin. Because reversal time and reversal duration are derived from the same fitted trajectory, we treat their correlation primarily as a descriptive kinematic relationship rather than as independent evidence for a particular physical mechanism. The robust observational result is that later-reversing stations exhibit broader reversal transitions and that the northern stations generally show longer transitions than the southern stations at comparable positions along the propagation axis (Figs. 6 and S7). The systematic north-south offsets of pre-reversal span, post-reversal span and the relation between reversal time and duration (Figs. 4c, 4d and 4e) suggest that the decay of postseismic processes and the growth of the locking signal are both slower in the north segment of Tohoku rupture (i.e., Sanriku region) than those of the south segment (i.e., offshore Ibaraki), and hence the time-dependency characteristics of segments in north and south of the rupture may be fundamentally different. The ratio of the two spans is generally below 1 (mostly 0.8 to 0.95; Fig. 4f), indicating that the pre-reversal span is slightly shorter than the post-reversal span, so the reversal transition is mildly asymmetric, with the approach to zero velocity somewhat more abrupt than the subsequent onset of landward motion. The longitudinal color gradient shows that the ratio also depends on trench-normal position within each region (Fig. 4f) and hence on the coseismic stress perturbation.

4. Further Discussion

4.1 Sensitivity of Reversal Time and Reversal Duration Estimates

We evaluate the effects of the displacement threshold and fitted trajectory model on the reversal estimates. Changing the displacement threshold from 1 to 2 mm produces nearly identical reversal times (Figure S12a), because the threshold defines tmin and tmax around the reversal but does not materially alter the zero crossing of the fitted velocity. We also replace the preferred linear-plus-logarithmic function with a quadratic function (Figure S12b). For stations that reversed within the observation period, the estimated reversal times remain close, with an RMSE of 1.192 year (Figure S12b). These comparisons indicate that the within-record reversal times are relatively stable with respect to the tested threshold and functional form.

The estimated reversal duration depends on both the fitted trajectory and the prescribed displacement threshold because tmin and tmax are determined from the shape of the fitted displacement trajectory. Increasing the threshold systematically lengthens the total reversal duration (Figures S9, S10 and S14a) and decreases the ratio of the pre-reversal to post-reversal spans (Figures S11, S12 and S14b). However, the post-reversal span remains longer than the pre-reversal span, and the relationship between reversal duration and reversal time retains a positive slope at all tested thresholds (Figure S14c). Thus, the absolute duration varies with the selected threshold, whereas the longer durations at later-reversing stations and the asymmetry around (tr) persist across the tested thresholds. We retain 1 mm as the reference threshold because it is comparable to the horizontal precision of the GNSS observations.

The two functions differ more strongly when used to extrapolate reversal times beyond the observations (Figure S13b). A quadratic displacement function imposes constant acceleration, whereas the transient velocity in the linear-plus-logarithmic function progressively decays with elapsed time. We therefore retain the linear-plus-logarithmic function for the preferred estimates shown in Figure S6, while treating estimates beyond the GNSS records as a model-dependent scenario.

4.2 Deformation Reversal as an Observational Constraint on Megathrust Relocking

Megathrust relocking following a great subduction earthquake can be directly inferred from the apparent reversal of crustal deformation on land, from pervasive seaward motion during the coseismic and early postseismic phases to landward motion as postseismic transients decay and the megathrust relocks (Wang et al., 2012; Bedford et al., 2016; Govers et al., 2018). For small to great subduction earthquakes (Mw < 8.5), the duration of this deformation reversal across the entire continental side is generally short, ranging from less than a few months to a couple of years (e.g., Rémy et al., 2016; Hoffmann et al., 2018; Hobbs et al., 2019; Hormazábal et al., 2023). This is because the seaward postseismic transient, driven by the limited rupture area and relatively small coseismic stress perturbations, is easily suppressed by the strong landward interseismic signal associated with broader-scale background megathrust locking (Li & Chen, 2023). For larger events, the postseismic transient is much stronger, and the full deformation reversal on the continental side takes much longer time and could only be inferred from snapshots of subduction zones that have hosted giant (M9) megathrust earthquakes and are now in different earthquake-cycle phases (Wang et al., 2012). The exact spatiotemporal evolution of deformation reversal following a giant event has therefore never been documented at any single margin, owing to the lack of dense modern geodetic observations of sufficient duration.

Previous modeling of inland postseismic GNSS observations together with seafloor GNSS-A observations, by independent groups, has reached a consensus that afterslip and viscoelastic mantle relaxation jointly contribute to the postseismic crustal deformation (e.g., Sun et al., 2014; Iinuma et al., 2016; Freed et al., 2017; Agata et al., 2019; Fukuda & Johnson, 2021; Dhar & Muto, 2023; Marsman et al., 2025). However, the lack of observations of the crustal deformation reversal itself hampers further precise and detailed mapping of when, where, and how afterslip vanishes and relocking initiates along the megathrust fault following a great rupture, and has led to simplified working assumptions in which the relocking signal is either ignored or the megathrust is assumed to relock immediately to its preseismic state after the great earthquake (e.g., Sun et al., 2018; Fukuda & Johnson, 2021). With decades of progress in understanding earthquake-cycle deformation, and now with observations of crustal deformation reversal in Japan and potentially in Sumatra and Maule Chile, we are well positioned to relax these assumptions and to better constrain the spatiotemporal evolution of megathrust relocking, and ultimately to advance our understanding of the megathrust re-healing process and the assessment of earthquake and tsunami hazard.

4.3 Implications for the Locking State of the Japan Trench

Given the persistent deformation reversal observed in the north and south (Figs. 3 and S6), we suspect that the 2025 burst of megathrust earthquakes offshore Aomori in the north (e.g., Zhang et al., 2026) may be related to the progressive crustal deformation reversal around 41°N and hence the broadly locked megathrust interface, whereas the reversal in southeastern Chubu-Kanto may be related to the complete decay of the significant afterslip and prevalent megathrust relocking directly observed by seafloor GNSS-A (e.g., Iinuma et al., 2016; Watanabe et al., 2021). In the central rupture area, the megathrust interface may feature enhanced relocking, similar to that observed in adjacent segments (Fig. 1) (Heki & Mitsui, 2013; Melnick et al., 2017; Yuzariyadi & Heki, 2021; D'Acquisto & Govers, 2023), in addition to the contribution of viscoelastic relaxation (e.g., Sun et al., 2014; Watanabe et al., 2021; Sun et al., 2024; Fang et al., 2025). Thus, the onshore deformation is mutually compatible with the offshore observations, and the two jointly suggest that the megathrust along the Japan Trench may have broadly relocked, at least in its shallow portion. This relocking, however, is far from uniform: the pronounced north-south contrast and the arcuate, decelerating reversal front indicate that it is spatially heterogeneous and cannot be simply modeled as a homogeneous process (Johnson et al., 2016; Mavrommatis et al., 2017; Johnson & Burton, 2026).

4.4 Observational Benchmarks for Coupled Earthquake-cycle Models

Rather than uniquely decomposing the surface observations into individual physical processes, the present dataset defines quantitative benchmarks that coupled earthquake-cycle models should reproduce. These include (1) the arcuate geometry of the reversal-time field, (2) the contrasting northward and southward kinematic migration rates and their temporal deceleration, (3) the broader reversal transitions at later-reversing stations and the systematic north-south offset in transition duration, and (4) the persistence of seaward motion in central Tohoku after 15 years. Simultaneously reproducing these features will provide a stronger test of coupled afterslip, viscoelastic relaxation, and renewed interseismic loading than fitting individual postseismic snapshots alone.

However, modeling these conjectures remains difficult, because fault relocking is expected to involve highly nonlinear and coupled processes along the plate interface and within the bulk rheology of the subduction system. The spatial pattern and timing of crustal deformation reversal documented in this study (Figs. 3 and S6) are unprecedented observations at subduction zones, and designing sophisticated three-dimensional models to fully and quantitatively explain them remains premature at this stage. Such models would require reasonable constraints on poorly known parameters, including the three-dimensional heterogeneous viscoelastic structure of both the oceanic and continental mantle (e.g., Freed et al., 2017; Suito, 2017; Li et al., 2018; Paul et al., 2024; Dhar et al., 2025; Marsman et al., 2025). Developing modeling frameworks that treat postseismic relaxation and interseismic relocking as coupled, simultaneous processes rather than sequential, independent ones (e.g., Li & Chen, 2023) is therefore a critical next step. Such three-dimensional forward

models, which investigate how the onset time, depth, and rate of relocking control the observed reversal pattern using the 15-year dataset presented here, are currently in preparation and will be the subject of a follow-up study.

5. Conclusions

Using more than 15 years of continuous GNSS observations across the Japanese islands, we document for the first time the spatiotemporal evolution of east-west surface deformation reversal following the 2011 Mw 9.1 Tohoku-Oki earthquake. The reversal initiates within one year near the southern and northern edges of the affected region and propagates toward central Tohoku as an arcuate surface-velocity zero contour. Central Tohoku remains dominated by seaward motion after 15 years, whereas the surrounding regions have progressively transitioned to landward motion. The two fronts advance at average velocities of 19.2 km/yr from the south and 13.3 km/yr from the north and decelerate systematically with time. The migration of this kinematic reversal front decelerates with time, although extrapolation beyond the GNSS record is strongly dependent on the assumed temporal function. The pre- and post-reversal time spans and the reversal duration are systematically larger in the northern segment than in the southern segment at a given distance along the propagation axis, and the reversal duration increases linearly with reversal time across the margin. The systematically longer transition durations in the north demonstrate distinct temporal characteristics of surface-deformation recovery between the Sanriku and offshore Ibaraki regions. The recent 2025 to 2026 burst of megathrust earthquakes in the Sanriku region (e.g., Yoshida et al., 2026; Zhang et al., 2026) and vanished afterslip inferred from GNSS-A offshore Ibaraki (Watanabe et al., 2021) occurred where our observations. Together, these observations provide a new margin-scale benchmark for models that seek to jointly reproduce afterslip, viscoelastic relaxation, and renewed interseismic loading during long-term megathrust healing.

Abbreviations

GEONET
GNSS Earth Observation Network System
GNSS
Global Navigation Satellite System
GNSS-A
Global Navigation Satellite System–Acoustic
GSI
Geospatial Information Authority of Japan
RMS
root mean square
RMSE
root-mean-square error

Declarations

Ethics approval and consent to participate

Not applicable.

Consent for publication

Not applicable.

Competing interests

The authors declare that they have no competing interests.

Authors' information

Authors and Affiliations

State Key Laboratory of Lithospheric Evolution, Institute of Geology and Geophysics, Chinese Academy of Sciences, Beijing, China

Xiaolong Zhang, Shaoyang Li & Ling Chen

College of Earth and Planetary Sciences, University of Chinese Academy of Sciences, Beijing, China

Xiaolong Zhang & Ling Chen

Funding

This work was supported by the National Key R&D Program of China (Grant No. 2023YFF0803200) and the National Natural Science Foundation of China (Grant No. 42288201).

Authors' contributions

S.L. conceived the original idea, which was elaborated on with X.Z, L.C. X.Z, S.L. conducted geodetic modeling. X.Z, S.L. prepared the figures and wrote the manuscript, with comments from L.C.

Acknowledgements

We thank Onno Oncken, Jun'ichi Fukuda, and Kosuke Heki for valuable discussions and encouragement, and Satoshi Ide, Anne Socquet, anonymous reviewers for comments on an earlier version of this paper.

Availability of data and materials

Daily GNSS displacement time series used in this study are available at the Nevada Geodetic Laboratory (http://geodesy.unr.edu/NGLStationPages/stations/) (Blewitt et al., 2018). All processed data will be made available at the time of publication via Zenodo at https://zenodo.org/records/20661851. In the meantime, they are available to reviewers at https://zenodo.org/records/20661851?preview=1&token=eyJhbGciOiJIUzUxMiJ9.eyJpZCI6IjRjMDQ0OWNkLTY4NDItNDJlNS04MzJmLTAzOWY3ODljMGFmOCIsImRhdGEiOnt9LCJyYW5kb20iOiJlNDn1y1U0EktYvnhxOngCTOgsFiAVCZOIb8vVJagHWCMWMu9AYRGqaWZHWiVXXTNxW_A___km2XTvig

References

1. Agata R, Barbot SD, Fujita K, Hyodo M, Iinuma T, Nakata R, Hori T (2019) Rapid mantle flow with power-law creep explains deformation after the 2011 Tohoku mega-quake. Nat Commun 10(1):1385. https://doi.org/10.1038/s41467-019-08984-7
2. Bevis M, Brown A (2014) Trajectory models and reference frames for crustal motion geodesy. J Geodesy 88(3):283–311. https://doi.org/10.1007/s00190-013-0685-5
3. Blewitt G, Hammond W, Kreemer C (2018) Harnessing the GPS data explosion for interdisciplinary science [Dataset]. Eos 99(2):e2020943118. https://doi.org/10.1029/2018eo104623
4. D'Acquisto M, Govers R (2023) Offshore landward motion shortly after a subduction earthquake implies rapid relocking of the shallow megathrust. Geophys Res Lett 50(1). https://doi.org/10.1029/2022gl101638. e2022GL101638
5. Dhar S, Muto J (2023) Function model based on nonlinear transient rheology of rocks: An analysis of decadal GNSS time series after the 2011 Tohoku-oki earthquake. *Geophysical Research Letters*, *50*(9), e2023GL103259. https://doi.org/10.1029/2023gl103259
6. Dhar S, Takada Y, Muto J (2025) Inferring 3-D rheology of low-viscosity zone around quaternary volcanoes of NE Japan from postseismic deformation of the 2011 Tohoku-Oki earthquake. J Geophys Research: Solid Earth 130(4):e2024JB029939. https://doi.org/10.1029/2024JB029939
7. Freed AM, Hashima A, Becker TW, Okaya DA, Sato H, Hatanaka Y (2017) Resolving depth-dependent subduction zone viscosity and afterslip from postseismic displacements following the 2011 Tohoku-oki, Japan earthquake. Earth Planet Sci Lett 459:279–290. https://doi.org/10.1016/j.epsl.2016.11.040
8. Fang J, Gurnis M, Mallick R (2025) Constraints on nonlinear mantle rheology from multi-scale geodetic observations of plate motion and post-seismic enhanced landward motion. Earth Planet Sci Lett 669:119566. https://doi.org/10.1016/j.epsl.2025.119566
9. Fukuda J, Johnson KM (2021) Bayesian Inversion for a Stress-Driven Model of Afterslip and Viscoelastic Relaxation: Method and Application to Postseismic Deformation Following the 2011 MW 9.0 Tohoku-Oki Earthquake. J Geophys Research: Solid Earth 126(5):e2020JB021620. https://doi.org/10.1029/2020jb021620
10. Govers R, Furlong KP, Van de Wiel L, Herman MW, Broerse T (2018) The geodetic signature of the earthquake cycle at subduction zones: Model constraints on the deep processes. Rev Geophys 56(1):6–49. https://doi.org/10.1002/2017RG000586
11. Heki K, Mitsui Y (2013) Accelerated pacific plate subduction following interplate thrust earthquakes at the Japan trench. Earth Planet Sci Lett 363:44–49. https://doi.org/10.1016/j.epsl.2012.12.031
12. Hobbs TE, Newman AV, Protti M (2019) Enigmatic upper-plate sliver transport paused by megathrust earthquake and afterslip. Earth Planet Sci Lett 520:87–93. https://doi.org/10.1016/j.epsl.2019.05.016
13. Honsho C, Kido M, Tomita F, Uchida N (2019) Offshore postseismic deformation of the 2011 Tohoku earthquake revisited: Application of an improved GPS-acoustic positioning method considering horizontal gradient of sound speed structure. J Geophys Research: Solid Earth 124(6):5990–6009. https://doi.org/10.1029/2018jb017135
14. Hormazábal J, Moreno M, Ortega-Culaciati F, Báez JC, Peña C, Sippl C, González-Vidal D, Ruiz J, Metzger S, Yoshioka S (2023) Fast relocking and afterslip-seismicity evolution following the 2015 Mw 8.3 Illapel earthquake in Chile. Sci Rep 13(1):19511. https://doi.org/10.1038/s41598-023-45369-9
15. Iinuma T, Hino R, Uchida N, Nakamura W, Kido M, Osada Y, Miura S (2016) Seafloor observations indicate spatial separation of coseismic and postseismic slips in the 2011 Tohoku earthquake. Nat Commun 7(1):13506. https://doi.org/10.1038/ncomms13506

16. Iwasaki T, Sato H, Shinohara M, Ishiyama T, Hashima A (2015) Fundamental structure model of island arcs and subducted plates in and around Japan. Agu Fall Meeting Abstracts 2015:T31B–T2878
17. Johnson KM, Burton ED (2026) Decadal Creep Acceleration on the Northern Japan Trench Driven by Erosion of. https://doi.org/10.22541/essoar.15006806/v1. Heterogeneously Locked Asperities
18. Johnson KM, Mavrommatis A, Segall P (2016) Small interseismic asperities and widespread aseismic creep on the northern Japan subduction interface. Geophys Res Lett 43(1):135–143. https://doi.org/10.1002/2015GL066707
19. Khazaradze G, Wang K, Klotz J, Hu Y, He J (2002) Prolonged post-seismic deformation of the 1960 great Chile earthquake and implications for mantle rheology. Geophys Res Lett 29(22):7–1. https://doi.org/10.1029/2002GL015986
20. Klotz J, Khazaradze G, Angermann D, Reigber C, Perdomo R, Cifuentes O (2001) Earthquake cycle dominates contemporary crustal deformation in Central and Southern Andes. Earth Planet Sci Lett 193(3–4):437–446. https://doi.org/10.1016/S0012-821X(01)00532-5
21. Li S, Chen L (2023) How long can the postseismic and interseismic phases of great subduction earthquake sustain? Toward an integrated earthquake-cycle perspective. *Geophysical Research Letters*, *50*(11), e2023GL103976. https://doi.org/10.1029/2023gl103976
22. Li S, Bedford J, Moreno M, Barnhart WD, Rosenau M, Oncken O (2018) Spatiotemporal variation of mantle viscosity and the presence of cratonic mantle inferred from 8 years of postseismic deformation following the 2010 Maule, Chile, earthquake. Geochem Geophys Geosyst 19(9):3272–3285. https://doi.org/10.1029/2018gc007645
23. Li S, Moreno M, Bedford J, Rosenau M, Heidbach O, Melnick D, Oncken O (2017) Postseismic uplift of the Andes following the 2010 Maule earthquake: Implications for mantle rheology. Geophys Res Lett 44(4):1768–1776. https://doi.org/10.1002/2016gl071995
24. Marsman CP, Vossepoel FC, D'Acquisto M, Van Dinther Y, van de Wiel L, Govers R (2025) Unraveling processes and rheology of the Tohoku earthquake cycle using bayesian inference. *Journal of Geophysical Research: Solid Earth*, *130*(5), e2024JB029665. https://doi.org/10.1029/2024JB029665
25. Mavrommatis AP, Segall P, Johnson KM (2017) A physical model for interseismic erosion of locked fault asperities. J Geophys Research: Solid Earth 122(10):8326–8346. https://doi.org/10.1002/2017JB014533
26. Melnick D, Moreno M, Quinteros J, Baez JC, Deng Z, Li S, Oncken O (2017) The super-interseismic phase of the megathrust earthquake cycle in Chile. Geophys Res Lett 44(2):784–791. https://doi.org/10.1002/2016gl071845
27. Nishimura T (2014) Pre-, co-, and post-seismic deformation of the 2011 Tohoku-oki earthquake and its implication to a paradox in short-term and long-term deformation. J Disaster Res 9(3):294–302. https://doi.org/10.20965/jdr.2014.p0294
28. Ozawa S, Nishimura T, Munekane H, Suito H, Kobayashi T, Tobita M, Imakiire T (2012) Preceding, coseismic, and postseismic slips of the 2011 Tohoku earthquake, Japan. J Geophys Research: Solid Earth 117:B7. https://doi.org/10.1029/2011jb009120
29. Puel S, Becker TW, Villa U, Ghattas O, Liu D (2024) Volcanic arc rigidity variations illuminated by coseismic deformation of the 2011 Tohoku-oki M9. Sci Adv 10(23):eadl4264. https://doi.org/10.1126/sciadv.adl4264
30. Rémy D, Perfettini H, Cotte N, Avouac JP, Chlieh M, Bondoux F, Sladen A, Tavera H, Socquet A (2016) Postseismic relocking of the subduction megathrust following the 2007 Pisco, Peru, earthquake. J Geophys Research: Solid Earth 121(5):3978–3995. https://doi.org/10.1002/2015jb012417
31. Sagiya T (2004) A decade of GEONET: 1994–2003 The continuous GPS observation in Japan and its impact on earthquake studies. Earth Planets and Space 56(8):xxix–xli. https://doi.org/10.1186/bf03353077
32. Simons M, Minson SE, Sladen A, Ortega F, Jiang J, Owen SE, Webb FH (2011) The 2011 magnitude 9.0 Tohoku-Oki earthquake: Mosaicking the megathrust from seconds to centuries. Science 332(6036):1421–1425. https://doi.org/10.1126/science.1206731
33. Suito H (2017) Importance of rheological heterogeneity for interpreting viscoelastic relaxation caused by the 2011 Tohoku-Oki earthquake. Earth Planets and Space 69(1):1–12. https://doi.org/10.1186/s40623-017-0611-9
34. Sun T, Wang K, He J (2018) Crustal deformation following great subduction earthquakes controlled by earthquake size and mantle rheology. J Geophys Research: Solid Earth 123(6):5323–5345. https://doi.org/10.1029/2017jb015242
35. Sun T, Wang K, He J (2024) Geodetic signature of a weak lithosphere-asthenosphere boundary in postseismic deformation of large subduction earthquakes. Earth Planet Sci Lett 630:118619. https://doi.org/10.1016/j.epsl.2024.118619
36. Sun T, Wang K, Iinuma T, Hino R, He J, Fujimoto H, Hu Y (2014) Prevalence of viscoelastic relaxation after the 2011 Tohoku-oki earthquake. Nature 514(7520):84–87. https://doi.org/10.1038/nature13778
37. Toda S, Stein RS (2022) Central shutdown and surrounding activation of aftershocks from megathrust earthquake stress transfer. Nat Geosci 15(6):494–500. https://doi.org/10.1038/s41561-022-00954-x
38. Tomita F, Kido M, Ohta Y, Iinuma T, Hino R (2017) Along-trench variation in seafloor displacements after the 2011 Tohoku earthquake. Sci Adv 3(7):e1700113. https://doi.org/10.1126/sciadv.1700113
39. Uchida N, Bürgmann R (2021) A decade of lessons learned from the 2011 Tohoku-Oki earthquake. Rev Geophys 59(2) e2020RG000713. https://doi.org/10.1029/2020rg000713
40. Wang K, Sun T, Brown L, Hino R, Tomita F, Kido M, Fujiwara T (2018) Learning from crustal deformation associated with the M9 2011 Tohoku-oki earthquake. Geosphere 14(2):552–571. https://doi.org/10.1130/ges01531.1
41. Wang K, Hu Y, He J (2012) Deformation cycles of subduction earthquakes in a viscoelastic Earth. Nature 484(7394):327–332. https://doi.org/10.1038/nature11032
42. Watanabe SI, Sato M, Fujita M, Ishikawa T, Yokota Y, Ujihara N, Asada A (2014) Evidence of viscoelastic deformation following the 2011 Tohoku-Oki earthquake revealed from seafloor geodetic observation. Geophys Res Lett 41(16):5789–5796. https://doi.org/10.1002/2014gl061134

43. Yoshida K, Uno M, Bassett D (2026) The 2025 Mw 7.6 Aomori-Oki megathrust sequence and a slip-parallel seismic belt to the trench. *Geophysical Research Letters, 53*(11), e2026GL122361. https://doi.org/10.1029/2026gl122361
44. Yuzariyadi M, Heki K (2021) Enhancement of interplate coupling in adjacent segments after recent megathrust earthquakes. Tectonophysics 801:228719. https://doi.org/10.1016/j.tecto.2021.228719
45. Zhang X, Li S, Shi J, Itoh Y, Zhang J, Kato A, Chen L (2026) The 2025 Mw 7.6 Aomori megathrust earthquake in northeast Japan: Failure of a structurally and rheologically bounded asperity beneath a cold mantle wedge. *Geophysical Research Letters*, *53*(14), e2026GL122179. https://doi.org/10.1029/2026GL122179
46. Zhang X, Li S, Chen L (2025) Unexpected megathrust slip evolution revealed by the 2024 Mw 7.1 and the 2025 Mw 6.8 Hyuga-nada earthquakes in southwest Japan. Earth Planet Sci Lett 662:119384. https://doi.org/10.1016/j.epsl.2025.119384

Figures

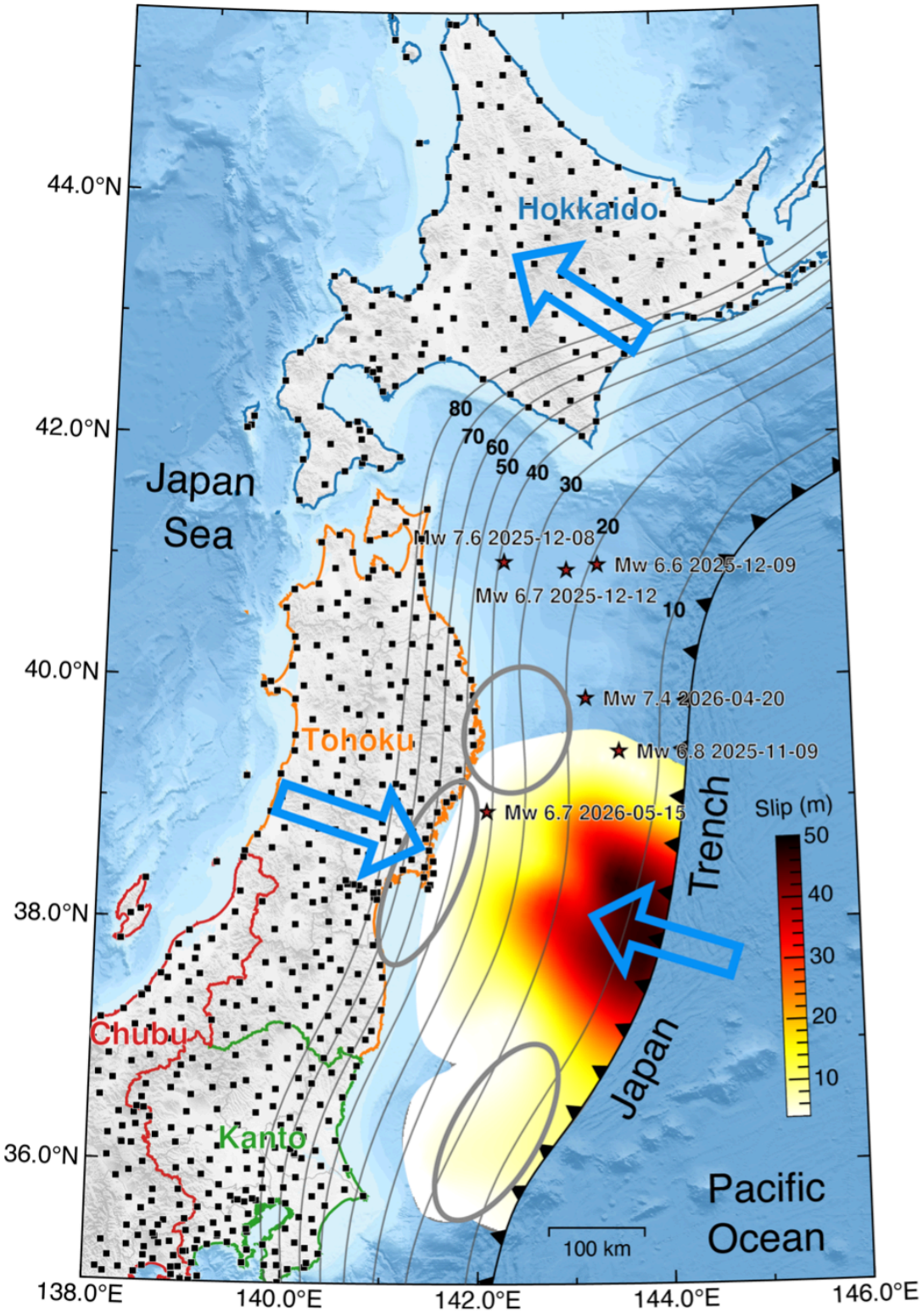

Figure 1

Seismotectonic settings of Japan Trench. Black squares denote the GEONET GNSS stations from Geospatial Information Authority of Japan used in this study (Sagiya, 2004). The coseismic slip distribution of the 2011 Tohoku-Oki earthquake is from Fukuda & Johnson (2021). Gray ellipses depict the rough locations of the possible afterslip from previous studies (e.g., Iinuma et al., 2016; Wang et al., 2018; Fukuda & Johnson, 2021). Blue hollow arrows show the overall contemporary deformation direction. Red stars mark the epicenters of seven Mw > 6.5 megathrust earthquakes that occurred between late 2025 and 2026 (Japan Meteorological Agency). Gray contours show plate-interface depth at 10-km intervals, based on the local slab model of Iwasaki et al. (2015).

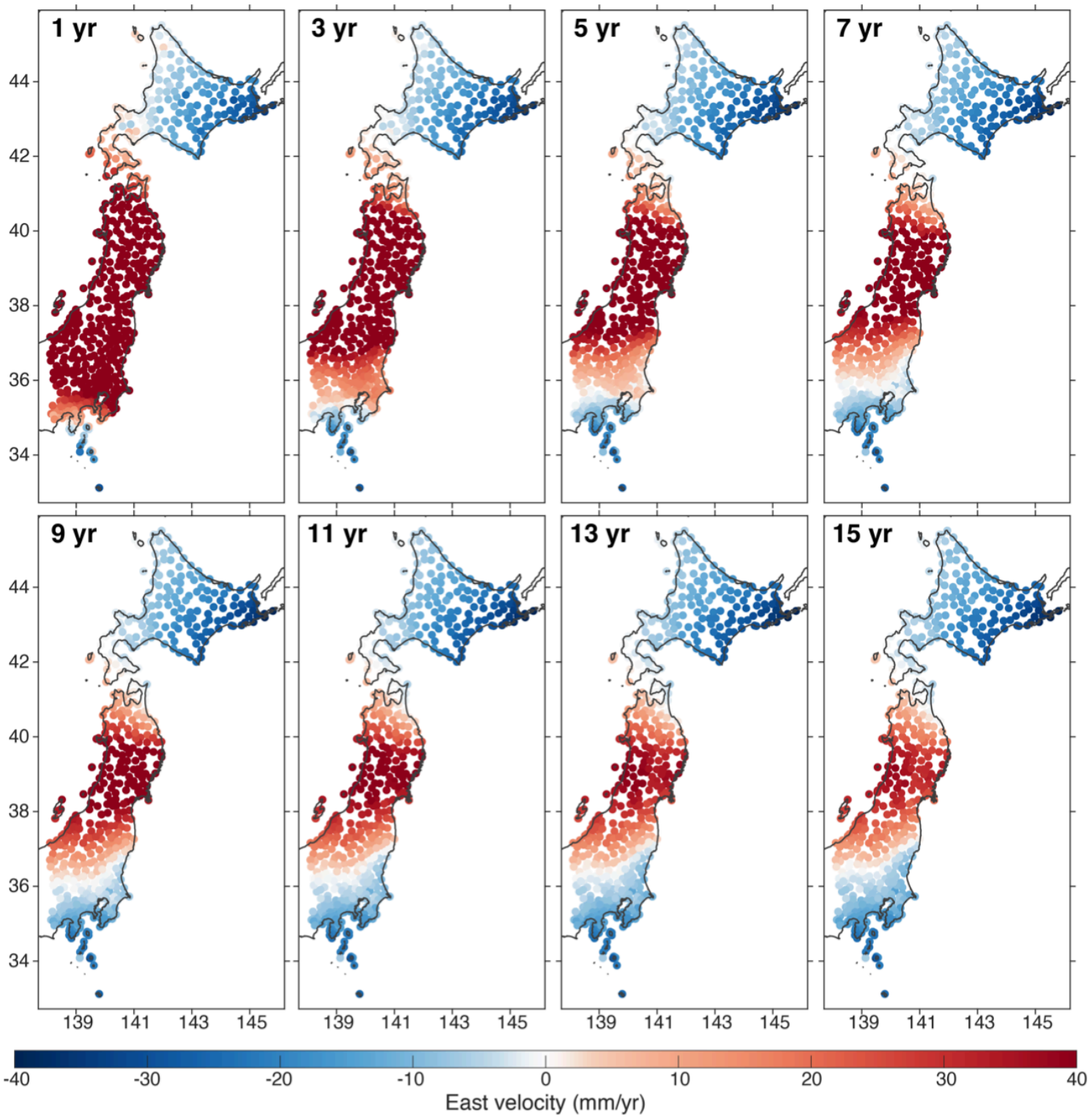

Figure 2

Spatial distribution of east-component velocities estimated from the fitted GNSS trajectories at different elapsed times as labeled in each panel since the 2011 Tohoku-Oki earthquake. Positive and negative values represent eastward and westward motion, respectively. Note that northeastern Hokkaido Island was not affected by the postseismic deformation of the 2011 event and shows persistent westward motion both before and after the earthquake.

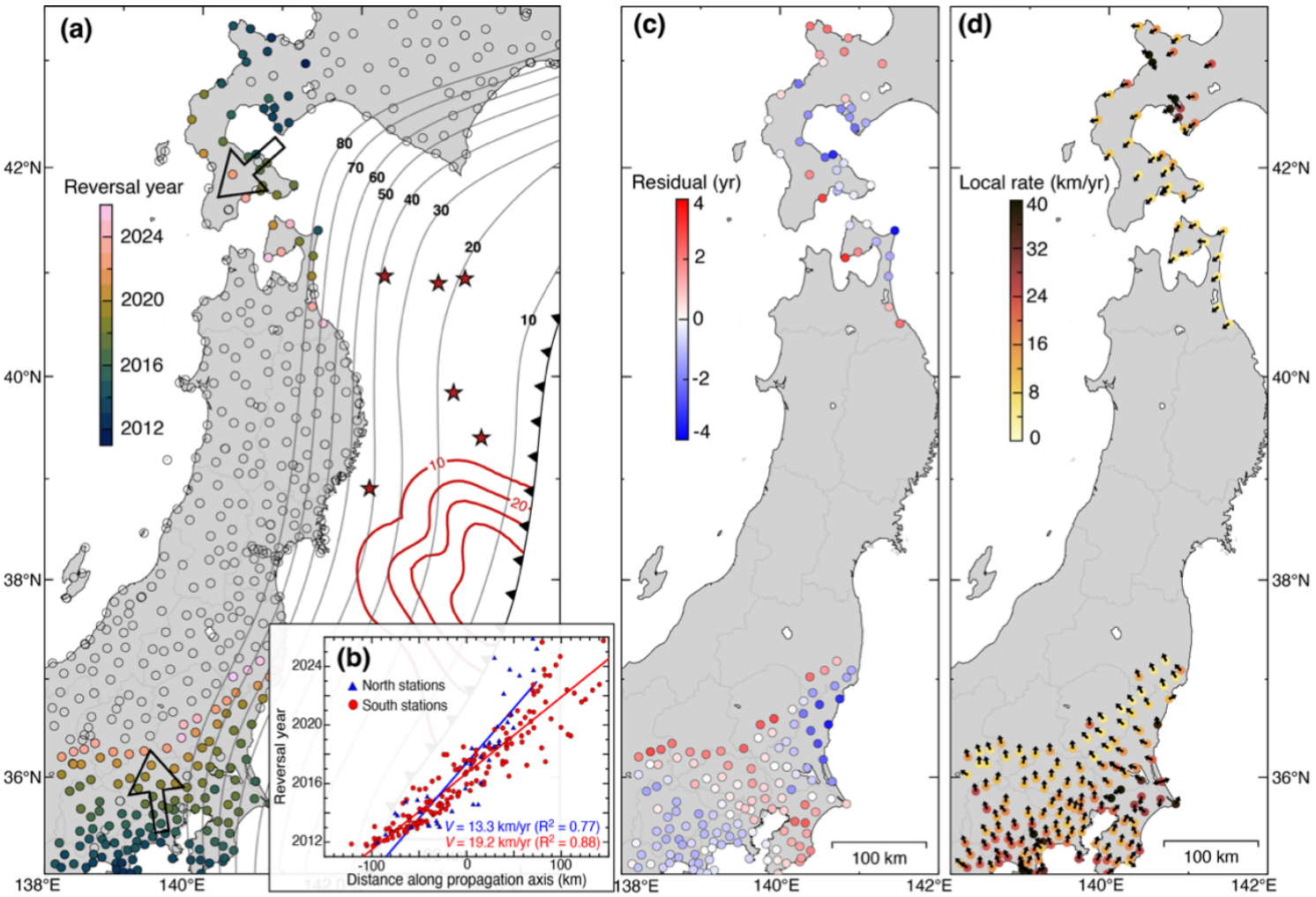

Figure 3

Observed east-west surface deformation reversal and its spatial propagation. **(a)** Reversed stations color-coded by reversal year and unreversed stations (open circles). Black open arrows show the propagation directions from planar fits to the reversed stations within the northern and southern regions. Red contours show the coseismic slip distribution of the Tohoku-Oki earthquake in 10 meters (Fukuda & Johnson, 2021). Red stars mark the epicenters of the 2025 to 2026 Mw > 6.5 megathrust events (Japan Meteorological Agency). **(b)** Reversal year against distance along the propagation axis for the northern stations and southern stations; solid lines are linear fits of these stations. **(c)** Residual reversal time (observed minus planar-fit prediction) at each reversed station. **(d)** Local propagation rate (color) and direction (arrows) at each reversed station.

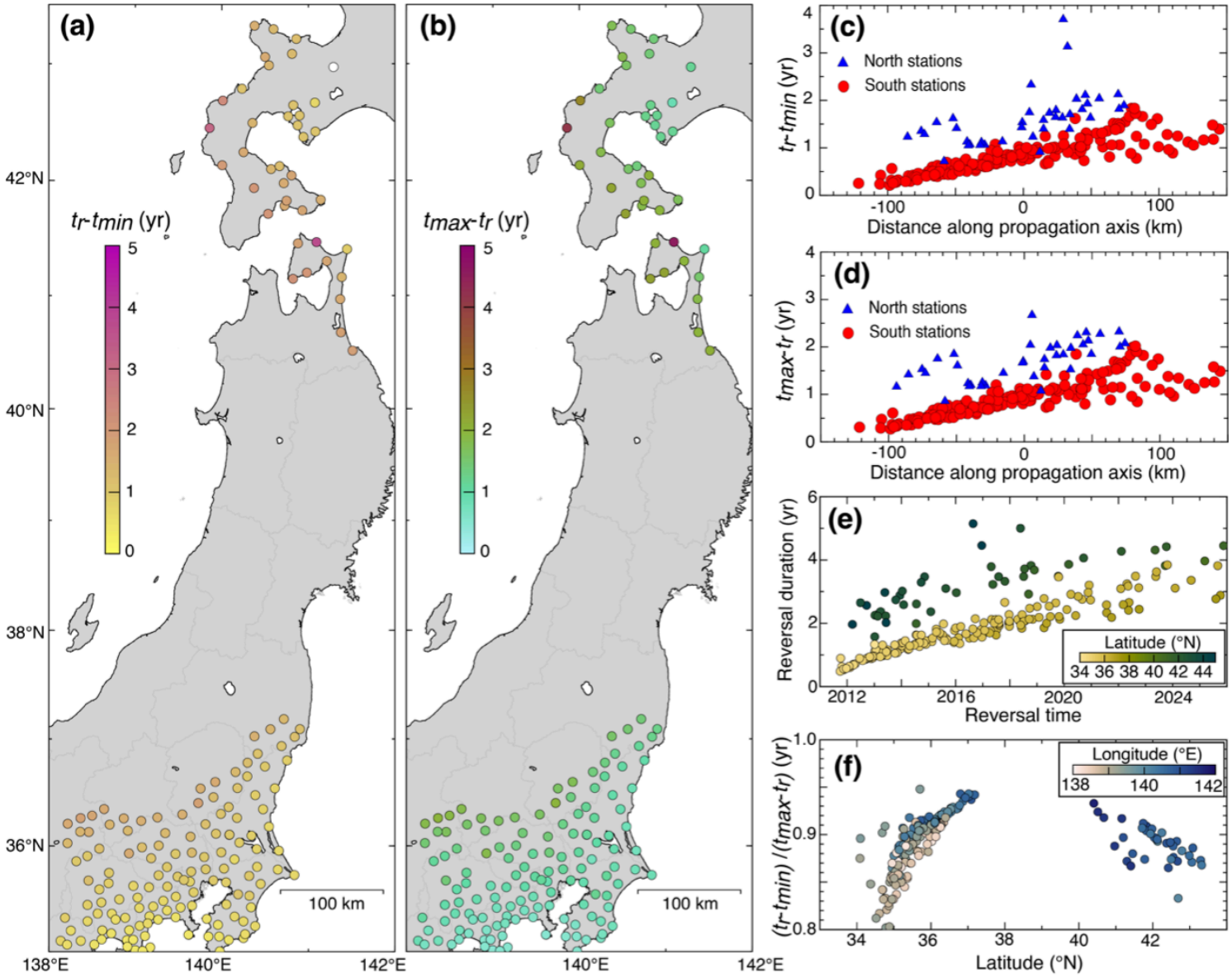

Figure 4

Spatiotemporal features of reversal durations at reversed stations. (a) Pre-reversal time span, tr - tmin. (b) Post-reversal time span, tmax - tr. (c) Pre-reversal time span against distance along the propagation axis for the northern stations (blue triangles) and southern stations (red circles). (d) Post-reversal time span against distance along the propagation axis, with symbols as in (c). (e) Reversal duration (tmax - tmin) against reversal time (tr), color-coded by latitude. (f) Ratio of the pre-reversal to post-reversal time span, (tr - tmin)/(tmax - tr), against latitude for all reversed GNSS stations, color-coded by longitude. Here tr is the reversal time, and tmin and tmax are the lower and upper bounds of the reversal transition defined by the 1 mm prescribed displacement tolerance.

Supplementary Files

This is a list of supplementary files associated with this preprint. Click to download.

- GraphicalAbstract.png
- SIclean.docx